Metastable droplets on shallow-grooved hydrophobic surfaces

Olesya Bliznyuk, Vasilisa Veligura, E. Stefan Kooij,* Harold J. W. Zandvliet, and Bene Poelsema
Physics of Interfaces and Nanomaterials, MESA+ Institute for Nanotechnology, University of Twente, Enschede, The Netherlands
(Received 23 December 2010; published 15 April 2011)

The equilibrium shapes of water droplets on shallow-grooved hydrophobic surfaces are studied experimentally. The dependence of the two final states, notably metastable Cassie-Baxter and Wenzel, on the underlying geometric pattern is analyzed and discussed. Surprisingly, in contrast to theoretical expectations, a significant portion of the droplets are in the Cassie-Baxter state. The anisotropy of the patterns, defined by the relative groove and ridge widths, allows studying the influence of different mechanisms of spreading in orthogonal directions on the final shape of the droplets. The validity of the Cassie-Baxter and Wenzel models in the case of anisotropic surfaces is investigated, comparing the experimental data with theoretical predictions in the two respective regimes. The influence of varying ridge widths for fixed groove widths on the final state adopted by the droplets, i.e., Cassie-Baxter or Wenzel, is discussed.

DOI: 10.1103/PhysRevE.83.041607 PACS number(s): 68.03.Cd, 68.08.Bc

I. INTRODUCTION

The behavior of liquids on surfaces, which have been modified in a controlled way both structurally and chemically, is of great interest from a theoretical as well as a practical point of view. Of particular interest are studies on "lotus leaf" or superhydrophobic surfaces, on which a liquid will have large contact angles (CAs) and roll off easily, making them exhibit self-cleaning properties [1–3]. The range of applications for these superhydrophobic surfaces extends from car windows to microfluidics. This in turn explains the amount of research dedicated to designing robust lotus surfaces as well as studying the behavior of liquid droplets they support. Despite the vast amount of work being carried out in this field of research, numerous questions remain unanswered regarding the influence of particular surface structures on the equilibrium shape as well as, especially, dynamic behavior of liquid drops.

Summarizing the experimental and theoretical research until now, on hydrophobic rough surfaces ($\theta_{St} > 90^\circ$) the liquid droplet can end up in two distinct equilibrium states: (i) the Wenzel state, in which all asperities are filled with liquid, or (ii) the "fakir" or Cassie-Baxter state, in which air pockets are trapped in the structures beneath the droplet. Both states effectively increase the apparent CA as denoted by θ_W or θ_{CB}, respectively, for the two aforementioned states. However, for the so-called lotus effect, the fakir state is required.

When a liquid fills all of the underlying structural features, there is a complete wetting of the liquid-solid interface. This leads to an increase of the total wetted area with respect to the flat surface. In this case the Wenzel equation [4] is used to estimate the apparent macroscopic CA θ_W:

$$\cos\theta_W = r\cos\theta_{St}, \tag{1}$$

where r is the roughness factor, defined as the ratio of the actually wetted surface to the projected flat area under the droplet; r is always greater than 1. The angle θ_{St} corresponds to the Young CA the liquid assumes on the same smooth, chemically homogeneous surface.

In the Cassie-Baxter or fakir state, the droplet rests on the tops of surface asperities, trapping pockets of air within the structure. The Cassie-Baxter equation [5] is used to estimate the apparent macroscopic CA θ_{CB} for a droplet on a composite surface consisting of air and a hydrophobic solid:

$$\cos\theta_{CB} = f_s(\cos\theta_{St} + 1) - 1. \tag{2}$$

Here f_s represents the fraction of the liquid interface that is in contact with the solid as compared to the projected surface area [6].

In a number of studies dealing with morphologically structured, hydrophobic surfaces, the Cassie-Baxter state appears to have a higher energy as compared to the Wenzel state. In other words, complete wetting of the surface structures corresponds to a situation of thermodynamic equilibrium. Nevertheless, the metastable Cassie-Baxter state is frequently observed on these surfaces due to the fact that the droplets are deposited from the top, effectively experiencing a local energy minimum [7–9]. The presence of an activation energy between metastable and thermodynamic equilibrium situations gives rise to droplets residing in the Cassie-Baxter state without spontaneous decay into the energetically more favorable Wenzel state. To gain insight on the transition mechanism, complete wetting of the structures can be induced by an increase of the Laplace pressure for example arising from evaporation [10,11], by application of an electric voltage [12], or vibrations [13]. Although various approaches, supported by experimental data, have been suggested to model the transition [14–20], the exact mechanism remains elusive.

The aforementioned studies of the relative stability of the Cassie-Baxter and Wenzel states, as well as the transition from one state to the other, are typically performed on well-defined, isotropically structured surfaces. Highly appealing are surfaces with an anisotropic pattern that favors spreading of liquid in certain directions and hindering spreading in other directions. This generally leads to static droplet shapes deviating from spherical ones. Understanding of droplet dynamics on such surfaces is of considerable interest both from a theoretical as well as an application point of view [21]. Anisotropic surfaces are abundant in nature [22,23]; their artificial equivalents with

*e.s.kooij@utwente.nl

 ©2011 American Physical Society

controlled structures can be used to study the occurrence of both states as well as their interdependence. Nevertheless, such studies prove to be rare owing to the difficulty to analyze the directional wetting characteristics. Consequently, the range of applicability of Cassie-Baxter and Wenzel equations in the case of anisotropic surfaces remains an open question. The most often investigated anisotropic surfaces consist of parallel grooves, being attractive for their relative simplicity in modeling the results and the wide range of possible applications. The studies are typically carried out either for complete wetting, i.e., systems in the Wenzel state [24–26], or for liquid droplets suspended on top of the grooves, i.e., the Cassie-Baxter state [27].

Here we present an experimental investigation into the behavior of liquid droplets on shallow groove-patterned hydrophobic surfaces. Calculations to estimate the relative stability of the Cassie-Baxter and Wenzel states using actual geometric parameters reveal that for all surfaces the equilibrium situation corresponds to the Wenzel regime. Nevertheless, we observe systematically that droplets adopt either Cassie-Baxter or Wenzel states depending on the underlying pattern. Furthermore, the influence of the anisotropic pattern on the final shape and macroscopic CAs are studied for both regimes and compared to what is expected on the basis of the aforementioned models.

II. EXPERIMENTAL DETAILS

A. Surface preparation

We prepare our surfaces using standard clean room methods as schematically shown in Fig. 1. First, the oxide layer is removed from the Si wafers to assure an identical thickness of native oxide, therewith providing better homogeneity between different batches of wafers. Next, freshly cleaned wafers are spin-coated with positive photoresist. Subsequently, the photoresist is soft baked and the pattern is transferred via standard optical lithography [Fig. 1(a)]. Once the exposed photoresist is washed off, the remaining photoresist is baked. The exposed Si regions are etched by reactive ion etching (RIE) [28]. Anisotropic etching is used to create well-defined profiles of grooves 2 μm deep [Fig. 1(b)]. After removing the photoresist, the depth and the homogeneity of the etching at different places on wafers are assessed using a profilometer (Veeco Dektak 8). Finally, the wafers are thoroughly cleaned in nitric acid to prepare for hydrophobization of the surface with a self-assembled monolayer (SAM) of 1H,1H,2H,2H-Perfluorodecyltrichlorosilane (PFDTS, 97%, ABCR, Germany) [Fig. 1(c)]. The assembly of molecules creates a densely packed thin layer with a height on the order of 1 nm, on which water has a static CA $\theta_{St} = 110^\circ$. On our experimental surfaces we measured static CA $\theta_{St} = 109^\circ$ (averaged over 8 independent measurements on flat parts of the wafer), confirming the good quality of our SAMs. Vapor deposition of the PFDTS molecules is done in a degassed chamber that is exposed in successive turns to PFDTS and water reservoirs to introduce the respective vapors, initiating the reaction on the wafer surface. Using a controlled environment ensures good quality and reproducibility of the SAMs [29].

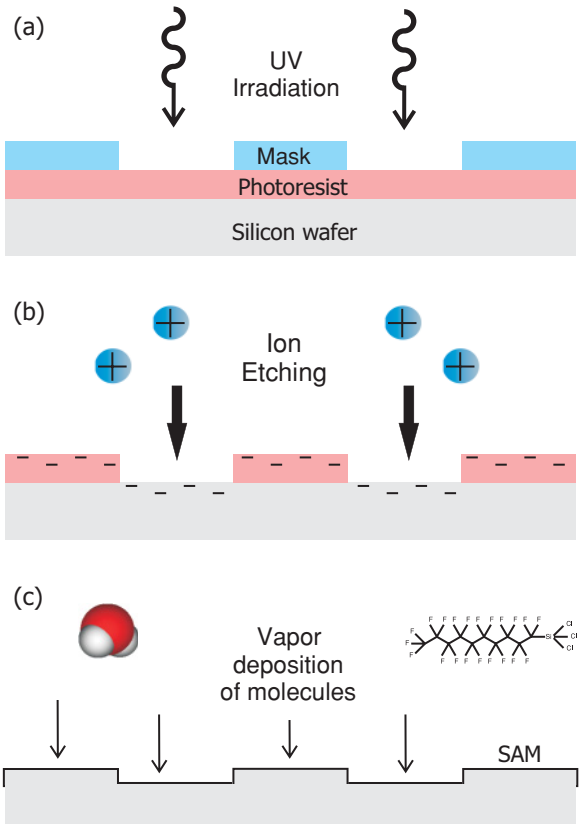

FIG. 1. (Color online) Schematic representation of the different surface preparation steps. (a) A photoresist layer on the Si wafer is exposed to light through a mask. Parts of the positive photoresist that are exposed to the light will be washed away, therewith creating a pattern on the surface. (b) Parts of the wafer that are not protected by photoresist will be removed by reactive ion etching (RIE) [28]. (c) After removal of the photoresist, a self-assembled monolayer of PFDTS is deposited. Wafers are placed in a glass chamber that is degassed below 50 mbar (vapor pressure of PFDTS). Subsequent steps are (i) the chamber is connected to a reservoir containing liquid molecules, introducing PFDTS; (ii) the chamber containing PFDTS vapor is connected to a water reservoir, introducing water vapor, initiating silanization on the surface of the wafers [29].

B. Droplet deposition

Droplet deposition and characterization, including measurements of CAs, is done using an OCA 15+ apparatus (DataPhysics, Germany). The equipment enables determination of CAs with as accuracy of 0.5°. Droplets are created using a computer-controlled syringe. The liquid used is high purity water (from a Millipore Simplicity 185 system). For all droplets the volume is fixed at 1 μl.

Deposition of droplets for part of the patterns (the relatively more hydrophilic substrates) is achieved by gentle lowering of a syringe with a suspended droplet until it contacts the surface. The droplet spreads on the surface while still remaining attached to the needle. The detachment from the needle is induced by manual retraction of the syringe. Due to the relatively small volume of droplets in our experiments, the gravitational influence can be neglected.

For other patterns (relatively more hydrophobic), gentle lowering of the syringe will give rise to spreading of the droplet

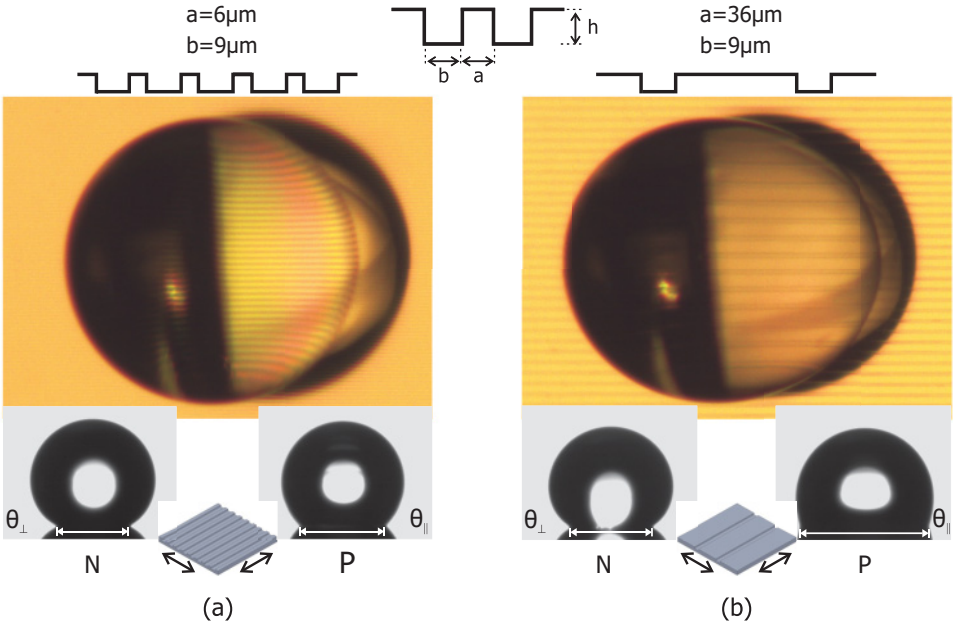

FIG. 2. (Color online) Water droplets on grooved surfaces, showing top-view images of the final droplet shape on two surfaces with identical groove width but different ridge width. At the top a schematic representation of our experimental surfaces is shown, defining relevant parameters a and b. (a) Droplet in the Cassie-Baxter state residing on a pattern with groove and ridge widths of 9 μm and 6 μm, respectively. The bright-yellow lines correspond to the empty grooves, while dark stripes correspond to ridges. The dimensions seen through the droplet (which acts as a lens) appear larger; this magnification is even more obvious in case of the Wenzel state. (b) Droplet in the Wenzel state for groove and ridge widths of 9 μm and 36 μm, respectively. The brightness contrast is limited due to the shallow groove depth ($h = 2$ μm). The ridge edges appear darker due to scattering of light there. At the bottom, side-view images of the droplets reveal the directionally dependent CAs ($\theta_\parallel$ and $\theta_\perp$) as well as the diameter of the wetted area in directions perpendicular and parallel (left and right, N and P, respectively, as shown in the schematic drawings) to the grooves.

due to the pressure applied by the needle. However, when the needle is retracted the droplet remains attached to the needle and detaches from the surface. In these cases, the deposition was done by dropping droplets from a low height.

An additional camera is mounted above the substrate to assess the final shape of the droplets. Using the reflected light, it is possible to see through the droplet and view the liquid interface with the solid; the droplet effectively works as a magnifying glass. This property can be used to confirm the final state of the droplet as the light reflects differently from water-solid and water-air interfaces; typical examples are presented in Fig. 2 and Fig. 6. In the Cassie-Baxter state [Fig. 2(a) and Fig. 6(a)] the air-liquid interfaces suspended above the grooves appear to be bright due to light scattering as compared to the dark liquid-solid interfaces of the contact regions. In the Wenzel state [Fig. 2(b) and Fig. 6(b)] the wetted area appears to have a more uniform color as the grooves are filled with liquid; the grooves appear to have a slightly darker shade as less light reflects from the sides of the grooves.

III. RESULTS

Depending on the ridge width, while keeping the groove width constant, the droplets end up in different static situations: Either the Cassie-Baxter or Wenzel states are adopted. As a general rule, for patterns with ridge widths smaller or equal to the width of the grooves, the final state adopted by the droplets is the Cassie-Baxter regime. As the ridge width becomes larger than the groove width, droplets end up in the Wenzel state.

An example of a droplet in the Cassie-Baxter state is presented in Fig. 2(a). The droplet has a spherical shape, reflecting little influence from the underlying anisotropic pattern. Indeed, the side-view images show that CAs ($\theta_\parallel$ and $\theta_\perp$) and diameters both perpendicular and parallel to the grooves (N, resp. P) have similar values.

The second set of photos [Fig. 2(b)] shows the droplet in the Wenzel state. From the top view, the elongation in the direction of the grooves can be observed, similarly to what was previously described for chemically patterned surfaces [21,30]. The side-view photos show the difference in CAs ($\theta_\parallel$ and $\theta_\perp$) and diameter lengths of the wetted area in orthogonal directions. The $\theta_\perp$ and N appear to have similar values to those of the droplet in the Cassie-Baxter state [compare Fig. 2(a)]. However, the $\theta_\parallel$ have markedly smaller values, and the length P is larger as for the droplet in the Cassie-Baxter state.

A. Droplet spreading parallel to the grooves

In Fig. 3 the CAs measured in the direction parallel to the grooves ($\theta_\parallel$) are presented. To illustrate the general trend, in Fig. 3(a) $\theta_\parallel$ for a set of patterns having the same groove width of 9 μm is plotted. As the plot reveals, $\theta_\parallel$ is maximum for the smallest ridge width of 3 μm; CA values decrease as the ridge width becomes larger. A similar trend for $\theta_\parallel$ is observed for all groove widths we investigated. The two final states observed are separated by the dotted line: The line is arbitrarily placed

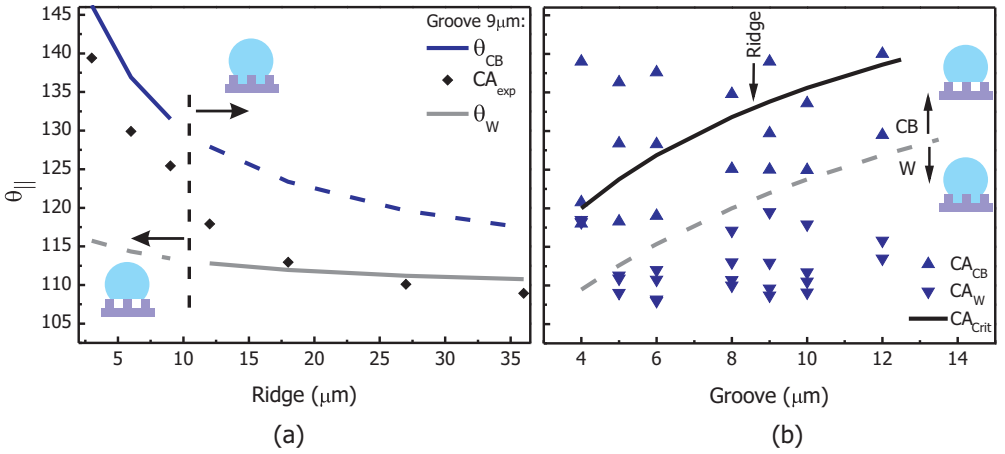

FIG. 3. (Color online) Experimental static water CAs measured in the direction parallel to the grooves ($\theta_\parallel$). All patterns have a groove depth of $h = 2$ μm. (a) Variation of $\theta_\parallel$ as a function of ridge width for patterns with groove width $b = 9$ μm. Solid lines represent theoretical curves for θ_{CB} (black line) and θ_W (gray line). The vertical dotted line indicates the separation between ridge values corresponding to the Cassie-Baxter state ($a < 9$ μm) and the Wenzel state ($a > 12$ μm). (b) $\theta_\parallel$ for all ridge widths studied, plotted as a function of groove width. For every groove width studied, the trend presented in (a) is observed; i.e. patterns with a ridge width smaller than the groove width are in the top part of the plot. Going from top to bottom in each column, the ridge width increases and consequently $\theta_\parallel$ decreases. The triangles indicate whether droplets are in the Cassie-Baxter (up triangle) or Wenzel (down triangle) state. The dashed and solid lines are discussed in the text.

between two experimentally studied ridge widths to indicate where the transition takes place. Furthermore, the $\theta_\parallel$ values can be compared to the isotropic θ_{CB} and θ_W calculated by inserting our experimental parameters into Eq. (1) and Eq. (2). As observed in the plot, the θ_{CB} values agree fairly well with the trend of the $\theta_\parallel$ for droplets suspended on the top of the ridges, although theoretical values are slightly higher. In the Wenzel regime, the values of θ_W are in better agreement with the $\theta_\parallel$ despite the fact that we are still dealing with anisotropy for which Eq. (1) is in principle not valid.

The static $\theta_\parallel$ values for all patterns included in this study are plotted in Fig. 3(b). The groove width is presented on the x axis: Each vertical column of data points corresponds to a single value for the groove width while the ridge widths are varied, enabling us to present all data in one single graph. The dotted line indicates the separation between two regions: In the upper part of the graph the droplets are in the Cassie-Baxter state, while in the lower part they are in the Wenzel regime. The distinct separation between the two regimes suggests a systematic dependence on the underlying pattern and allows us to use existing equations to account for the results.

In Fig. 4(a) and Fig. 4(b) we plot $\theta_\parallel$ as a function of scaling parameters characteristic for each regime. We use the solid fraction $f_s = a/(a+b)$ to plot the data for Cassie-Baxter state, while in the Wenzel state the groove-to-ridge ratio b/a is employed following Patankar's suggestion [15]. Although there is no rigorous theoretical background for using the groove-to-ridge ratio as scaling parameter, trends exhibited by experimental data are most pronounced when the ratio b/a is employed. Equally, theoretical θ_{CB} and θ_W values are plotted, which have been calculated assuming a circular shape of the contact area.

In the Cassie-Baxter regime [Fig. 4(a)] the $\theta_\parallel$ values appear to scale to a single line as a function of the solid fraction f_s, following the trend predicted by Eq. (2). Such behavior can be seen as a supplementary confirmation of the regime the droplets are in. The systematically lower experimental values may be due to a slight elongation of the wetted area in the direction of the grooves, resulting in aspect ratios $\xi = P/N$ (defined as the ratio of length P and width N; see Fig. 2) between 1.2 and 1.4 [see Fig. 4(c)]. Another reason for observing smaller $\theta_\parallel$ values may arise from the way the droplets are deposited on the surface. Previously, it has been observed that releasing droplets from a small altitude leads to lower contact angles due to the kinetic effects [8].

In the Wenzel regime [Fig. 4(b)], the $\theta_\parallel$ appear to scale as a function of the groove-to-ridge ratio b/a. Despite the fact that the roughness r is a scaling parameter for the Wenzel regime, using it for plotting masks the trend observed in the experimental data. Both $\theta_\parallel$ and θ_W values increase with b/a ratio, although the trends are different. For the $\theta_\parallel$, the patterns with low b/a ratios exhibit the lowest CAs with values similar to the θ_{St} on the flat surface. As the b/a ratio, and thus the number of grooves under the droplet, increases, so does $\theta_\parallel$, until it reaches a maximum value of 120°. The trend predicted by the Wenzel equation [Eq. (1)], shown by the black dots in Fig. 4(b), also exhibits a rise of θ_W with b/a, but less pronounced as compared to the experimental data. The reason for the relatively small variation of calculated θ_W values lies in the shallow depth of the grooves (2 μm). For ratios b/a below approximately 0.3, i.e., patterns having large ridge widths compared to the grooves, the $\theta_\parallel$ are smaller than θ_W. For the b/a ratio around 0.5, theory and experiment exhibit similar values. Once the ratios exceed 0.6, i.e., when the ridge width approaches the groove width, the calculated θ_W values are smaller than the $\theta_\parallel$.

Furthermore, the values of $\theta_\parallel$ measured in the Wenzel regime for $b/a > 0.6$ are similar to those exhibited in the Cassie-Baxter regime for solid fractions f_s between 0.6 and 0.7, corresponding to situations in which the ridge is slightly

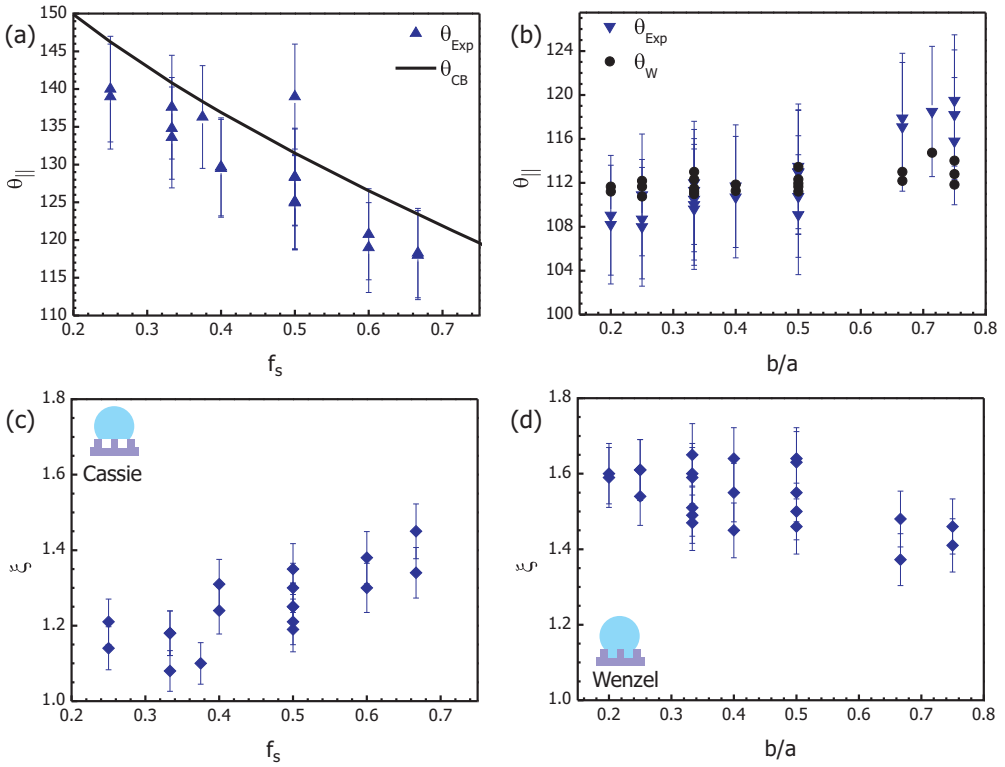

FIG. 4. (Color online) Top panels show experimental $\theta_{\parallel}$ values of the droplets. (a) $\theta_{\parallel}$ in the Cassie-Baxter regime as a function of solid fraction f_s [$f_s = a/(a+b)$]. The theoretical θ_{CB} is given by the solid line. (b) $\theta_{\parallel}$ in the Wenzel regime as a function of groove-to-ridge ratio b/a. Theoretical θ_W values are represented by the black dots. More than one calculated CA value for a single b/a ratio are due to roughness $r = (a+b+2h)/(a+b)$ definition. In our experiments, several groove/ridge combinations corresponding to a single b/a ratio, give slightly different r values. We choose to plot θ_W as function of b/a ratio and not the scaling parameter of the Wenzel regime, i.e., roughness r, as plotting CAs versus roughness does not exhibit a clear trend. Droplet aspect ratios are shown in the bottom panels for the Cassie-Baxter (c) and Wenzel (d) regimes.

larger than the groove, as can be seen from Fig. 4(a). Such elevated $\theta_{\parallel}$ values in the Wenzel regime may be explained based on the observation that, despite the deposition of the droplets via gentle lowering (characteristic of liquid filling the underlying structures), they tend first to reside for a short period of time in the partial Cassie-Baxter state (see also Fig. 6). Spontaneous collapse into the energetically more favorable Wenzel state always occurs within seconds. More details pertaining to the kinetics of droplet deposition are presently under investigation and are considered beyond the scope of this report.

To study the influence of the anisotropic pattern on the final shape and to quantify the distortion from a spherical shape, the aspect ratios ξ for droplets in both regimes are plotted in Fig. 4(c) and Fig. 4(d). To identify trends in the experimental data, the ξ values are plotted as a function of groove-to-ridge ratio b/a in the Wenzel regime, while in the Cassie-Baxter regime the solid fraction f_s is used to present the data.

In the Cassie-Baxter regime, the final shape of the droplets shows a relatively small deviation from a spherical geometry due to the underlying anisotropic pattern. For small f_s, i.e. when the droplet is primarily suspended over the air pockets between the ridges, the final shape is almost spherical, showing only a very slight elongation in the direction of the grooves ($\xi \approx 1$). As the solid part in contact with the droplet increases, the influence of the pattern on the final shape becomes more pronounced with ξ increasing to reach values of 1.4 for $f_s > 0.5$. Furthermore, both diameters parallel P and perpendicular N to the grooves become larger as f_s increases.

The highest experimental ξ values are observed in the Wenzel regime, reaching maximum values of approximately 1.6 [Fig. 4(d)]. Considering that the $\theta_{\parallel}$ values for these substrates are nearly equal to those on a flat surface [Fig. 4(b)], it seems that the elongation cancels an increase of $\theta_{\parallel}$ due to the grooves beneath the droplet. As the groove-to-ridge ratio b/a increases, the ξ decreases to finally scatter around 1.4. Interestingly, all droplets in the Wenzel regime have N values scattering around 0.85 mm; the observed trend for ξ is governed solely by the variation of the droplet length P (see Fig. 5).

B. Droplet spreading perpendicular to the grooves

The $\theta_{\perp}$ and N trends allow a better assessment of equilibrium shapes. Other than presenting a very different behavior compared to the results in the direction parallel to the grooves, they provide a more profound indication of similarities between the regimes (in the case of $f_s > 0.5$ and $b/a > 0.5$). In Fig. 5 the apparent macroscopic CAs $\theta_{\perp}$ in the direction perpendicular to the grooves [Fig. 5(a) and Fig. 5(b)]

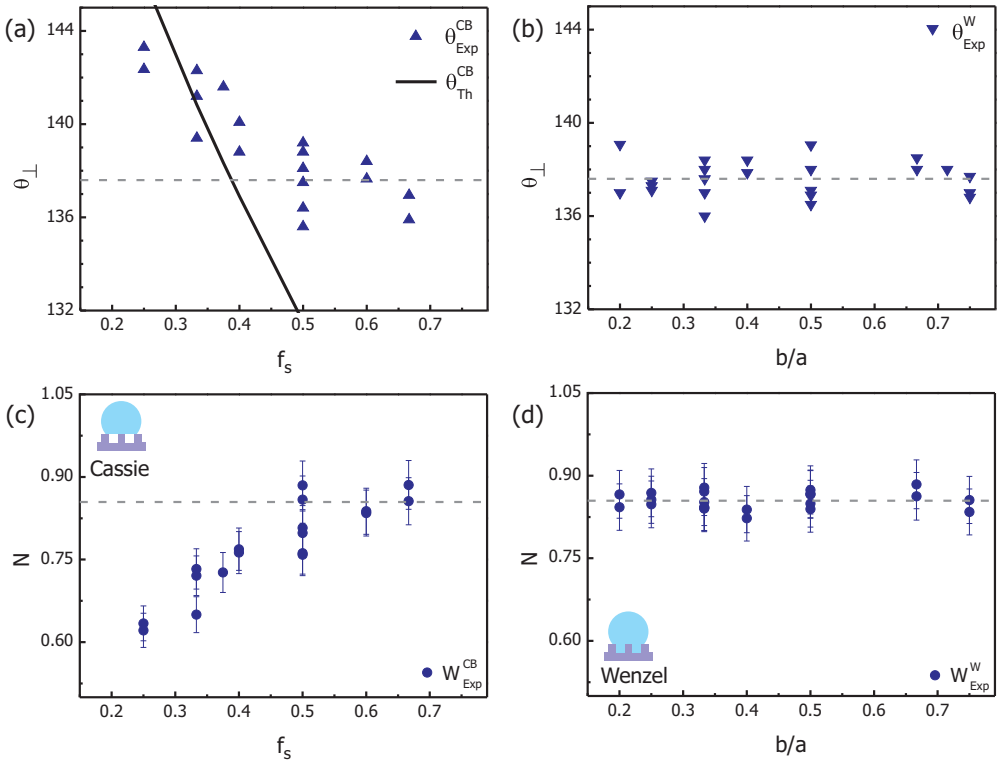

FIG. 5. (Color online) Top panels show experimental $\theta_\perp$ values of the droplets. (a) $\theta_\perp$ in the Cassie-Baxter regime as a function of solid fraction f_s [$f_s = a/(a+b)$]. Theoretical θ_{CB} is plotted as solid line to show that only part of the data seem to follow the model predictions. (b) $\theta_\perp$ in the Wenzel regime as a function of groove-to-ridge ratio b/a. The values scatter around 137.6° for all patterns studied. Bottom panels show the evolution of the wetted area diameter measured perpendicular to the stripes N for the Cassie-Baxter (c) and Wenzel (d) regimes.

and the diameter N of the wetted area [Fig. 5(c) and Fig. 5(d)] are plotted as a function of f_s (Cassie-Baxter regime) and b/a ratio (Wenzel regime).

In the Wenzel regime $\theta_\perp$ [Fig. 5(b)] scatters around a mean value of 137.6° for all patterns considered in this work; equally, the droplet diameters N scatter around 0.85 mm [Fig. 5(d)]. Such independence of the final dimensions on the underlying pattern, especially for large b/a ratio, would suggest a similar spreading mechanism close to reaching the static shape. As mentioned previously, for $b/a > 0.5$ parts of the droplet remain suspended and the grooves are filled within seconds after deposition. Given the same CA and N values, it would mean that the filled or empty state of the grooves away from the border of the droplet has little influence on the static values in the direction perpendicular to the grooves.

In the Cassie-Baxter regime [Figs. 5(a) and 5(c)] for $f_s < 0.5$, the $\theta_\perp$ decrease as f_s increases as well as exhibit values that are similar to $\theta_\parallel$; this is to be expected since the droplets have a spherical geometry with low ξ values close to 1.2 [see Figs. 4(a) and 4(c)]. The diameter N of the wetted area also becomes larger as f_s increases in agreement with the variation of CA values. In short, for $f_s < 0.5$ the behavior expected for droplets in Cassie-Baxter regime is observed.

Moreover, such limited influence of the underlying pattern with small f_s on the final shape in case of the Cassie-Baxter final state is of interest by itself. Previously reported spherically shaped droplets on anisotropic microscaled [22] or grooved [31] surfaces are attributed to high roughness of surfaces on both microscopic and nanoscopic scales, which is not the case for our experimental surfaces. For droplets suspended on the smooth ridge tops, the distortion of the contact area that follows the underlying structure is observed [27,32]. Moreover, the suspended state appears to be stable and the spontaneous transition into the energetically more favorable Wenzel state does not take place. Given the shallowness of the structures, the stability may be attributed to the pinning of the contact line on the edges of the ridges [33].

However, for $f_s > 0.5$ the values do not show any dependence on the underlying pattern: $\theta_\perp$ scatters around a value of 137.6° and N scatters around 0.85 mm. The same behavior as well as similar values are observed for the droplets in the Wenzel regime. Studying of the top-view images of droplets reveals no filled grooves in the regions close to the edge of the droplets. Comparing experimental results for different groove widths reveals identical values of $\theta_\perp$ and N once the ridge width exceeds 8 μm, suggesting that the width of the grooves has very limited or no influence at all. Moreover, combined with the similarity to the results for droplets in the Wenzel regime on patterns with $b/a > 0.5$, where the grooves near the edge of the droplet are filled, it can be reasoned that the filled or empty state of grooves is not the parameter that influences the static shape in this case.

IV. DISCUSSION

In the previous section we have described our observations pertaining to droplets on morphologically stripe patterned surfaces. Depending on the relative ridge and groove widths, droplets adopt either the Cassie-Baxter or Wenzel state. In this section we first discuss the observations in relation to energetic considerations. Next, we focus on the main issue of the present work, i.e., the transition from the metastable Cassie-Baxter to the Wenzel state as a function of ridge width.

A. Final state of droplets: Theoretical predictions

As described in the introduction, on low surface energy substrates in which liquid has static CAs $\theta_{St} > 90^\circ$ generally two states are observed when the surface exhibits roughness: the Wenzel or Cassie-Baxter state. Using energy arguments, one can calculate the apparent CAs in both regimes for a given rough surface. Direct comparison of calculated θ_{CB} and θ_W for a given surface allows evaluation of the relative stability of the two states: The regime exhibiting a smaller macroscopic apparent CA corresponds to a lower energy state and should be preferentially adopted by the liquid. Plotting the cosines of both θ_{CB} and θ_W as a function of substrate roughness presents a simple way to identify whether either the Cassie-Baxter or the Wenzel state corresponds to the thermodynamic equilibrium as well as gives an indication of the energy barrier separating the two states. Generally, if droplets end up in the fakir state on a surface where the Wenzel regime is energetically more favorable, the droplets are said to be in the metastable Cassie-Baxter state. Furthermore, the intersection point between the two regimes, corresponding to surface structures when both states have the same energy and, consequently, the same apparent CA, can be calculated.

A relatively simple way to predict *a priori* which state should be adopted on a given hydrophobic structured surface was suggested by Quéré [7,33]. If the roughness r and solid fraction f_s are known, the critical CA θ_{Cr} for a flat surface with similar properties can be calculated:

$$\cos\theta_{Cr} = \frac{1 - f_s}{r - f_s}. \tag{3}$$

Comparing θ_{St} measured on flat surface with calculated θ_{Cr} estimates which of the two is more likely to be adopted. If θ_{St} on the flat surface is smaller than θ_{Cr} ($\theta_{St} < \theta_{Cr}$), than the Wenzel state is energetically more favorable. Otherwise, the Cassie-Baxter or fakir state corresponds to the situation with minimum energy. In our case for grooved surfaces the roughness r is given by [4]

$$r = \frac{a + b + 2h}{a + b}, \tag{4}$$

where h is the depth of the grooves, fixed to 2 μm. Inserting this, together with $f_s = a/(a + b)$, into Eq. (3), we obtain the following expression for θ_{Cr}:

$$\cos\theta_{Cr} = \frac{-1}{1 + \frac{2h}{b}}. \tag{5}$$

We find that the critical angle is independent of the ridge width a but only depends on the groove width b and the ridge height h. A similar dependence solely on pitch width and height of the structures has been described for other geometries [8,34,35].

The resulting values for θ_{Cr} are represented in Fig. 3(b) by the solid black line, changing from 120° for a groove width of 4 μm to 138.6° for a groove width of 12 μm. On the unpatterned PFDTS treated silicon wafer we measure the $\theta_{St} = 109^\circ$ which makes $\theta_{St} < \theta_{Cr}$ for all studied patterns. Consequently, the Cassie-Baxter state does not correspond to the minimum energy situation for all surfaces considered in our present work. Most likely, the reason why we indeed observe this metastable state on a number of patterns is related to the way the droplets are deposited on the surface, i.e., by dropping them from a certain height [7,8]. However, that does not account for the Cassie-Baxter state stability on our experimental surfaces.

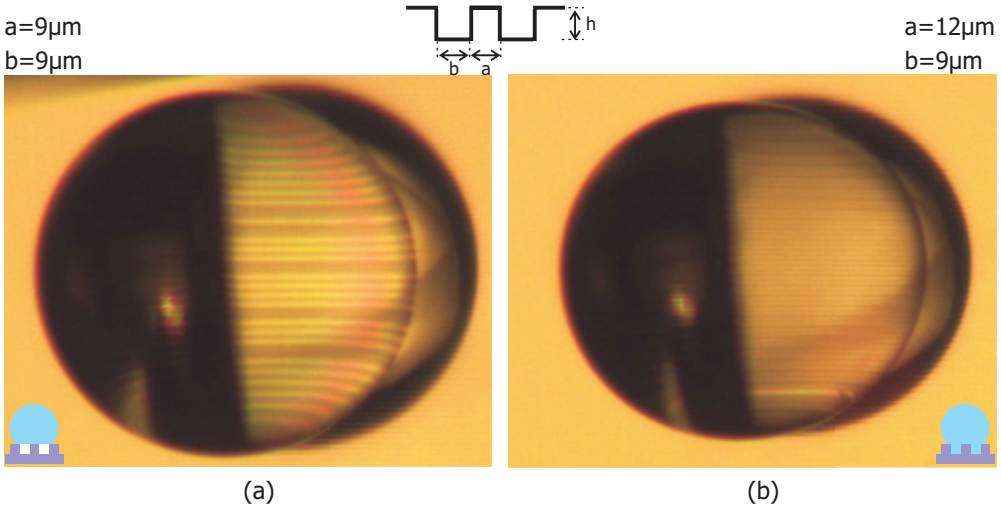

FIG. 6. (Color online) Snapshots of droplets observed on surfaces with (a) $f_s = 0.5$ (Cassie-Baxter regime) and (b) $b/a = 0.75$ (Wenzel regime). In both regimes the droplets appear to have almost spherical shapes irrespective of the way the droplets were deposited on the surface.

Further, the calculated θ_{Cr} [Fig. 3(b), solid line] for all groove widths appears to follow a similar trend as, although are systematically larger than, the border region between patterns on which the metastable Cassie-Baxter state is observed and patterns where droplets are in the Wenzel state. Moreover, calculations for the critical θ_{Cr} agree well with the experimentally observed transition from one regime to the other when the height-to-groove width ratio in the denominator in Eq. (5) is multiplied by a factor of 2 [Fig. 3(b), gray dashed line]. This correction holds for all experimental sets studied, although the origin of this multiplication factor is unclear. Apart from the qualitative agreement, the aforementioned model, which has been nicely described by Bico et al. [14], seems to somehow be in qualitative agreement with our observations; why this is the case for our anistropic grooved surfaces is unclear.

B. Transition from metastable Cassie Baxter to stable Wenzel

Returning to the data presented in Fig. 4 and Fig. 5, on a fraction of the patterns where the groove and ridge widths are equal or very close (i.e., in the case of $f_s > 0.5$ and $b/a > 0.5$), both states seem to exhibit similar values for the CAs and diameters of the wetted area. As an illustration in Fig. 6 two snapshots are shown of droplets, one being mostly suspended on the grooves [Fig. 6(a)] while another almost completely fills the underlying structures [Fig. 6(b)]. The droplets ending up in the Wenzel state are initially in a partial Cassie-Baxter state leaving a number of grooves under the droplet not filled. Almost immediately, these collapse into the Wenzel state. The same happens if the droplets are dropped from a low height.

It appears that the patterns considered here are near the critical point where both states have the same energies and, supposedly, the transition between states occurs. On the patterns where the Cassie-Baxter state is observed, the energy barrier is just high enough to hinder the transition, while for the other patterns the transition barrier to the Wenzel state is low, allowing the droplets to go easily into the energetically more favorable situation from the metastable suspended state they are deposited in. Moreover, theoretically estimated critical points between filled and suspended states do not correlate with the experimentally observed transition, which possibly is the result of the anisotropy of the patterns.

To understand the liquid behavior on these patterns near the critical point, we can use the existing knowledge of contact line motion in both regimes. Summarizing, in the case of the Wenzel state, prior to filling of the next groove the advancing CA condition at the edge of the ridge has to be met. Once the dynamic CA at the edge reaches a value lower than the advancing CA, the droplet remains pinned and spreading in the direction perpendicular to grooves stops [24,36]. In the Cassie-Baxter state, the advancing edge of the droplet "falls" until it reaches the top of the neighboring ridge at the location corresponding to the area with the largest curvature of the droplet. Subsequently, it will advance over this next ridge if the condition of the advancing CA for a flat surface is met [17]. In both cases, the contact line will be pinned on the edge of the ridge before the next groove is bridged.

Assuming that both suspended and filled states have very similar energies and, consequently, exhibit similar values for macroscopic θ_{CB} or θ_W values, it is safe to suppose that the microscopic dynamic angles reach values prohibiting further advancing for similar macroscopic lengths. However, the width of the ridge should be large enough (in our case >8 μm), for similar N and $\theta_\perp$ in both regimes irrespective of the last groove "bridged" by the droplet being filled with liquid or whether the droplet remains suspended above it.

Considering the similar values for P and $\theta_\parallel$ observed on these surfaces (Fig. 4), the explanation most likely lies in the fact that droplets in the Wenzel state have not achieved their minimum energy shape. In the suspended state, the advancing contact line advances over the composite surface of air and hydrophobic solid, encountering a low energy barrier, resulting in static $\theta_\parallel$ values close to the ones predicted by Cassie-Baxter equation. For the filled state, the complete filling of the underlying structures occurs at later stages, the first shape being to a certain degree defined by spreading over the composite surface. Once the entire transition to the Wenzel state has taken place, it is possible that the microscopic condition for the advancing CA is no longer fulfilled and further filling of grooves to achieve lower macroscopic apparent CA is not possible. That would explain the experimental $\theta_\parallel$ exhibiting larger values as compared to the ones estimated by the Wenzel equation.

V. CONCLUSION

We have studied the equilibrium droplet behavior on anisotropic shallow grooved surfaces. The groove geometry creates two orthogonal spreading directions with different properties, resulting in elongated droplets with directionally dependent properties. From the experimental results, we find that two states are reproducibly observed on the studied anisotropic surfaces: (i) metastable Cassie-Baxter and (ii) Wenzel states, the latter corresponding to the thermodynamic equilibrium on our surfaces. Comparison between experimental $\theta_\parallel$ and θ_{CB} and θ_W predicted by theoretical equations reveals a similar trend but systematically lower values for droplets in the Cassie-Baxter regime. In the Wenzel regime, there is no agreement in trend. The elongation in the direction of the grooves is more pronounced for the Wenzel regime, while in the Cassie-Baxter regime the influence of the underlying pattern on the deviation of the droplet shape from a spherical geometry is much less pronounced. The energy barrier between the suspended state as compared to a complete filling of the underlying structures is low on a fraction of patterns, resulting in a spontaneous transition from the Cassie-Baxter to Wenzel state. Moreover, elevated values for $\theta_\parallel$ in the Wenzel state are observed. Finally, calculating the stability condition for both thermodynamically stable Cassie-Baxter and Wenzel states on surfaces with well-defined structures, we find that calculated θ_{Cr} values seem to agree with the transition trend between patterns observed for apparent θ_{CB} and θ_W.

ACKNOWLEDGMENTS

The authors thank James Seddon, University of Twente, for helpful discussions. We thank Patrick Jansen for helping with data processing. We gratefully acknowledge the support by MicroNed, a consortium to nurture microsystems technology in The Netherlands.

[1] C. Neinhuis and W. Barthlott, Ann. Bot. **79**, 667 (1997).
[2] X. M. Li, D. Reinhoudt, and M. Crego-Calama, Chem. Soc. Rev. **36**, 1350 (2007).
[3] J. Genzer and K. Efimenko, Biofouling **22**, 339 (2006).
[4] R. N. Wenzel, Ind. Eng. Chem. **28**, 988 (1936).
[5] A. B. D. Cassie and S. Baxter, Trans. Faraday Soc. **40**, 546 (1944).
[6] M. A. Raza, E. S. Kooij, A. van Silfhout, and B. Poelsema, Langmuir **26**, 12962 (2010).
[7] D. Quéré, A. Lafuma, and J. Bico, Nanotechnology **14**, 1109 (2003).
[8] B. He, N. A. Patankar, and J. Lee, Langmuir **19**, 4999 (2003).
[9] Y. C. Jung and B. Bhushan, J. Microsc. **229**, 127 (2008).
[10] G. McHale, S. Aqil, N. J. Shirtcliffe, M. I. Newton, and H. Y. Erbil, Langmuir **21**, 11053 (2005).
[11] M. Sbragaglia, A. M. Peters, C. Pirat, B. M. Borkent, R. G. H. Lammertink, M. Wessling, and D. Lohse, Phys. Rev. Lett. **99**, 156001 (2007).
[12] F. Mugele and J.-C. Baret, J. Phys. Condens. Matter **17**, R705 (2005).
[13] E. Bormashenko, R. Pogreb, G. Whyman, Y. Bormashenko, and M. Erlich, Appl. Phys. Lett. **90**, 201917 (2007).
[14] J. Bico, U. Thiele, and D. Quéré, Colloids Surf. A **206**, 41 (2002).
[15] N. A. Patankar, Langmuir **19**, 1249 (2003).
[16] A. Marmur, Langmuir **19**, 8343 (2003).
[17] C. W. Extrand, Langmuir **18**, 7991 (2002).
[18] M. Nosonovsky and B. Bhushan, Langmuir **24**, 1525 (2008).
[19] S. Moulinet and D. Bartolo, Eur. Phys. J. E **24**, 251 (2007).
[20] A. M. Peters, C. Pirat, M. Sbragaglia, B. M. Borkent, M. Wessling, D. Lohse, and R. G. H. Lammertink, Eur. Phys. J. E **29**, 391 (2009).
[21] O. Bliznyuk, H. P. Jansen, E. S. Kooij, and B. Poelsema, Langmuir **26**, 6328 (2010).
[22] L. Feng, S. H. Li, Y. S. Li, H. J. Li, L. J. Zhang, J. Zhai, Y. L. Song, B. Q. Liu, L. Jiang, and D. B. Zhu, Adv. Mater. **14**, 1857 (2002).
[23] Y. M. Zheng, X. F. Gao, and L. Jiang, Soft Matter **3**, 178 (2007).
[24] H. Kusumaatmaja, R. J. Vrancken, C. W. M. Bastiaansen, and J. M. Yeomans, Langmuir **24**, 7299 (2008).
[25] J. Y. Chung, J. P. Youngblood, and C. M. Stafford, Soft Matter **3**, 1163 (2007).
[26] D. Y. Xia, X. He, Y. B. Jiang, G. P. Lopez, and S. R. J. Brueck, Langmuir **26**, 2700 (2010).
[27] W. Choi, A. Tuteja, J. M. Mabry, R. E. Cohen, and G. H. McKinley, J. Colloid Interface Sci. **339**, 208 (2009).
[28] H. Jansen, H. Gardeniers, M. de Boer, M. Elwenspoek, and J. Fluitman, J. Micromech. Microeng. **6**, 14 (1996).
[29] H. Rathgen, Ph.D. thesis, University of Twente, 2008.
[30] O. Bliznyuk, E. Vereshchagina, E. S. Kooij, and B. Poelsema, Phys. Rev. E **79**, 041601 (2009).
[31] X. F. Gao, X. Yao, and L. Jiang, Langmuir **23**, 4886 (2007).
[32] Y. Chen, B. He, J. Lee, and N. A. Patankar, J. Colloid Interface Sci. **281**, 458 (2005).
[33] D. Quéré, Rep. Prog. Phys. **68**, 2495 (2005).
[34] B. Bhushan, M. Nosonovsky, and Y. Jung, in *Nanotribology and Nanomechanics*, edited by B. Bhushan (Springer, Berlin, 2008), pp. 995–1072.
[35] D. Bartolo, F. Bouamrirene, E. Verneuil, A. Buguin, P. Silberzan, and S. Moulinet, Europhys. Lett. **74**, 299 (2006).
[36] P. G. de Gennes, Rev. Mod. Phys. **57**, 827 (1985).